Drug Delivery and Translational Research (2023) 13:2394–2406
https://doi.org/10.1007/s13346-023-01323-w

ORIGINAL ARTICLE

Sustained-release behavior and the antitumor effect of charge-convertible poly(amino acid)s drug-loaded nanoparticles

Zhuang Hu[1] · Gongshu Wang[1] · Rui Zhang[1] · Yingyu Yang[2] · Jiwei Wang[2] · Jianshe Hu[1] · Aikebaier Reheman[3]

Accepted: 28 February 2023 / Published online: 13 March 2023

Abstract

Enhancing tissue permeability and achieving drug aggregation is the key to targeted tumor therapy. A series triblock copolymers of poly(ethylene glycol)-poly(L-lysine)-poly(L-glutamine) were synthesized by ring-opening polymerization, and charge-convertible nano-delivery system was constructed by loading doxorubicin (DOX) with 2-(hexaethylimide) ethanol on side chain. In normal environment (pH = 7.4), the zeta potential of the drug-loaded nanoparticle solution is negative, which is conducive to avoiding the identification and clearance of nanoparticles by the reticulo-endothelial system, while potential-reversal can be achieved in the tumor microenvironment, which effectively promotes cellular uptake. Nanoparticles could effectively reduce the distribution of DOX in normal tissues and achieve targeted aggregation at tumor sites, which can effectively improve the antitumor effect, while would not causing toxicity and damage to normal body.

Keywords Poly(amino acid)s · Drug delivery · Charge-conversion · Nanoparticles · Doxorubicin

Introduction

Cancer has become a major disease that threatening human health [1]. How to effectively control and conquer malignant tumors has become an urgent problem [2]. Chemotherapy is one of the main clinical means at present; however, conventional drugs may bring uncontrollable hurt to normal tissues, which limits the therapeutic field of drugs [3–5]. Compared with normal tissue, tumor microenvironment has unique properties [6–8], such as hypoxia, vascular abnormalities, high interstitial hydraulic pressure, immune inflammatory response, high lactate concentration, and low pH. In addition, proteoglycans and collagens can secrete a variety of extracellular matrices, including growth factors and inflammatory mediators, resulting in close communication between the tumor and the microenvironment, which poses a great challenge for drug delivery to the tumor [9, 10].

According to the specificity of tumor microenvironment, more and more nano-drug delivery systems with targeted and sustained release characteristics have been developed [11]. It has good clinical development value in improving the solubility of drugs, promoting the distribution and accumulation in tumor tissues, and improving the cellular uptake [12]. Compared with traditional chemotherapy, drugs in the nano-delivery system are encapsulated into the interior of the carrier, which can enhance the stability and improve the bioavailability [13–15]. In addition, because of the small size and good dispersion, nanoparticles can successfully penetrate the membrane for drug delivery by means of enhanced permeability and retention (EPR) effect. More importantly, nanocarriers can be functionalized to respond to various microenvironments and achieve targeted delivery [16].

Among a range of responsive stimuli, pH sensitivity, dependent on the tumor microenvironment, has been studied the most detailed [17, 18]. The pH value of normal body environment is maintained at about 7.4. Due to the high glycolysis rate of tumor cells, the value is reduced to 6.2–6.8,

✉ Jiwei Wang
jlwjw@sina.com

✉ Jianshe Hu
hujs@mail.neu.edu.cn

[1] Center for Molecular Science and Engineering, College of Science, Northeastern University, Shenyang 110819, People's Republic of China

[2] Present Address: Fujian Key Laboratory of Toxicant and Drug Toxicology, Medical College, Ningde Normal University, Ningde, Fujian 352100, People's Republic of China

[3] Present Address: Fujian Province University Engineering Research Center of Mindong She Medicine, Medical College, Ningde Normal University, Ningde, Fujian 352100, People's Republic of China

and the interior of cell endosomes/lysosomes is 4.5–5.5. The pH gradient is often used to design acid-triggered nano-drug delivery systems [19]. The surface of biofilms is negatively charged, and positively charged nanoparticles can be effectively captured and ingested [20, 21]. However, cationic nanoparticles are easily adsorbed by serum proteins and accumulate in organs such as the lung, liver, and spleen, which limits the application. Polymers containing tertiary amines can undergo the transformation of protonation or deprotonation when pH changes, and can perform charge reversal under acidic conditions to promote cellular uptake and achieve targeted release.

Poly(amino acid)s are a series of functional material that possess amphiphilic properties obtained by the polymerization of one or more amino anhydrides [22–24]. It has been being used in more and more fields due to its good degradability and biocompatibility [25–27]. Lysine [28] is an essential nutrient that helps the body produce antibodies, hormones, and enzymes. In addition, as an alkaline amino acid, the amino group on side chain provides active sites for chemical bonding to other compounds. Glutamic acid [29] is one of the basic amino acids for nitrogen metabolism in organisms, which is of great significance in tissue repair and other aspects. In this study, triblock copolymers of poly(ethylene glycol)-poly(L-lysine)-poly(L-glutamine) were synthesized and functionalized in the polyglutamic acid chain segment. The stability of the structure was proved by related tests. The nanoparticles bonded with doxorubicin (DOX) could have charge-convertible property in specific environment and could be effectively taken up by cancer cells with good antitumor effect. Safety assessment in vivo was confirmed by relevant histological analysis.

Experimental

Materials

Relevant solvents and compounds have been recrystallized or purified prior to use and are displayed in S1 (support information).

Characterization methods

The structure of products was characterized by Fourier transform infrared (FT-IR) spectra, ^{1}H nuclear magnetic resonance spectra (^{1}H-NMR) spectra, and gel permeation chromatography (GPC). The test of nanoparticles mainly includes UV–vis, dynamic light scattering (DLS), and transmission electron microscope (TEM). Cell and animal models used laser confocal microscopy (CLSM) and fluorescence microscope (see support information S2).

Ring-opening polymerization

Compounds containing amino groups can be used to initiate the reaction to synthesize poly(ethylene glycol)-poly(L-lysine)-poly(L-glutamine). In this experiment, $mPEG_{113}$-NH_2 was used as the initiator [26]. The main synthesis route is as shown in Scheme 1. L-Lys-NCA (0.612 g, 0.002 mol) was dissolved in 10 mL of dry DMF and transferred to a single ended flask. After that, the system is vacuumized and replaced with argon for three times to keep the system in an inert gas atmosphere. $mPEG_{113}$-NH_2 (1 g, 0.0002 mol) was dissolved in 10 mL of DMF and slowly injected into the reaction system. After continuous reaction at 30 °C for 72 h, L-Glu(OBzl)-NCA (0.526 g, 0.002 mol) was dissolved in 8 mL of DMF and slowly injected into the flask as the second stage of reaction. The overall process was stopped after continuous stirring for 72 h. The solution was concentrated to a suitable concentration by vacuum distillation, and a white powder solid, named P1-pro, was settled with diethyl ether as an undesirable solvent. The other two block polymers (P2-pro, P3-pro) were synthesized in the same way, except that the dosage of L-Glu(OBzl)-NCA was adjusted according to the proportion of the molecular design.

Removal of benzyl oxycarbonyl and benzyloxy

The hydrolysis reaction caused by the breaking of the amide bond or ester group under acidic conditions can achieve the removal of the protective group on the side chain. Herein, P1-pro (0.6 g) was dissolved in 10 mL of trifluoroacetic acid (TFA). Fifty minutes later, HBr/ACOH (5 mL) was added to the reaction flask. The whole system was kept in a closed state and stirred for 2 h at room temperature. Diethyl ether was used as an undesirable solvent to precipitate the target product (P1), which was a yellowish powdery solid. The other two (P2 and P3) were obtained by the same method.

Grafting of tertiary amine groups

P1 (0.94 g, 0.000116 mol) was dissolved in 10 mL of dry DMF, with DCC (0.478 g, 0.00232 mol) and DMAP (0.0004 mol, 0.05 g) were also added to the reaction bottle in an ice bath until the end of dripping. The activation of carboxyl group was achieved by stirring at room temperature for 5 h. N-(2-hydroxyethyl) hexa methylene imine (NHM) (0.332 g, 0.00232 mol) was diluted with DMF and injected slowly into the reaction system. The reaction lasted for 48 h at 35 °C. The by-product was removed by filtration, the solution was concentrated, and yellow solid was settled out by diethyl ether, which was named P1-NHM. P2-NHM and P3-NHM are obtained by changing the feeding ratio of NHM.

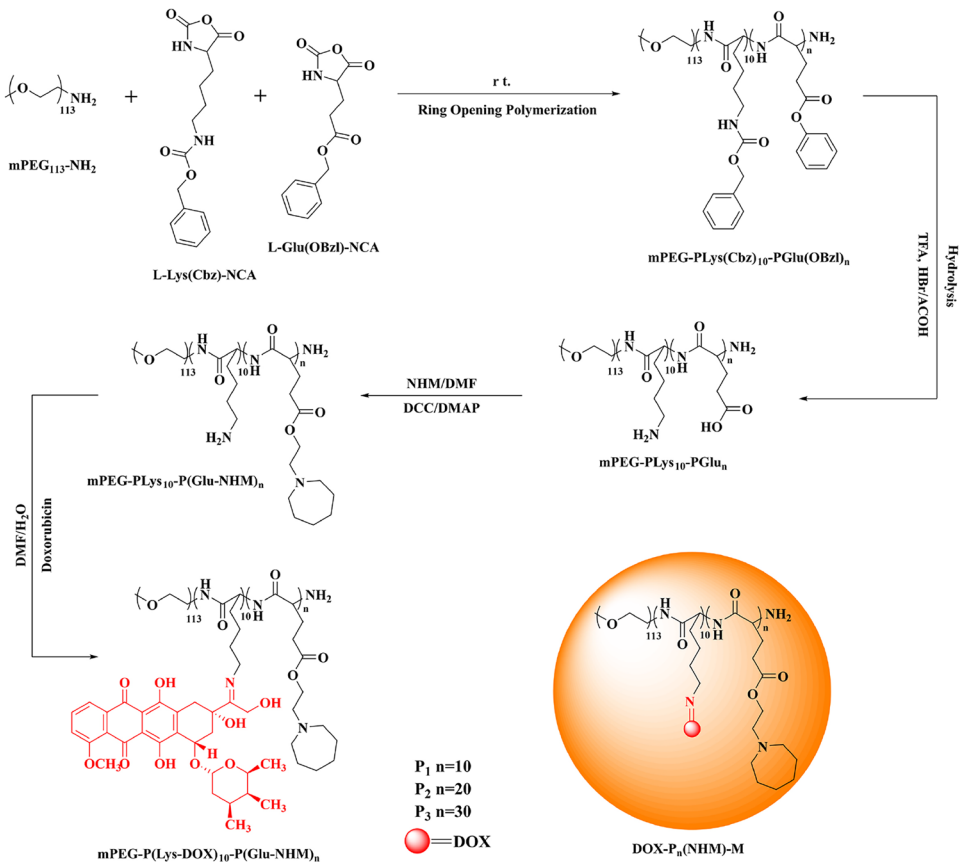

Scheme 1 Synthesis of poly(amino acid)s and principles of drug loading

Drug loaded process of polymers

Drug-loaded nanoparticles were obtained by nanoprecipitation method, and the final loading of model drug (DOX) could be achieved by physical embedding and chemical bonding. Herein, DOX·HCl (8 mg) was adequately dissolved in 5 mL of DMSO. Seven microliters of triethylamine was dripped into the conical flask and keep stirring for 6 h to achieve the removal of hydrochloric acid. Fifty milligrams of polymer (Pn-NHM) was respectively dissolved in 20 mL of anhydrous DMF and slowly injected into each of the conical flasks. The chemical bonding of DOX was achieved by continuously stirring for 24 h under the condition of avoiding light. Ten milliliters of PBS solution with pH = 7.4 was added into the flask so that more drugs were wrapped inside of macromolecules by self-assembly. Excessive DOX in the solution was removed by dialysis. Finally, the micellar solution was filtered via a 0.45-μm water phase filter membrane to remove precipitation and impurities, and DOX-Pn(NHM)-M was obtained. The relevant loading content (LC) and loading efficiency (LE) test methods of DOX are described in detail in S3 (support information).

Sustained-release in vitro

The concentrated nanoparticle solution was placed in dialysis bag and transferred to centrifuge tube. PBS buffer solution was added into each sample tube, and the pH of each group was adjusted to 5.0, 6.2, and 7.4, respectively. The system temperature was set to 37 °C and the constant speed of 100 rpm was continuously oscillated for 90 h. Within the set time, 3.5 mL of buffer solution was used to measure the absorbance of DOX, and the cumulative drug release rate at each sampling site was calculated according to the standard curve and regression equation. In another experimental inquiry, the temperature was set at 25 °C, 37 °C, and 45 °C, respectively, and pH = 7.4 was treated as invariant; the other operations were similar as before. The relevant formula see support information S4. The absorbance intensity at 505 nm was tested for all samples. Each data was measured three times in parallel and averaged.

Cytotoxicity of polymers and antitumor effect in vitro

The synthesized poly(amino acid)s were co-cultured with L929 cells to evaluate the cytocompatibility. In addition,

the cell inhibition effect of nanoparticles was studied by co-culture with Hela cells. The IC_{50} value can be calculated in accordance with the survival rate of cells after 24-h co-culture, and the cell uptake behavior can be observed by CLSM via resetting the co-culture concentration. See support information S5 for the relevant operation process.

Drug distribution in vivo

Animals and tumor models

Female Balb/C mice (18 ± 2 g, 5–6 weeks) were normally fed in the setting environment of 25 °C and 50–60% humidity; the light and dark surroundings were adjusted every 12 h. After 10 days, the animal model was established. Hela cells in the logarithmic growth were digested and collected into a centrifuge tube equipped with PBS. Cells were resuspended and blown evenly; 100 μL of suspension (1×10^7 cells) was injected subcutaneously into dorsal part of mice. The next experiment was carried out when the volume of tumor reached about 50 mm^3. All animal experiments were approved by the Northeastern University Medical Ethics Committee.

Biodistribution

According to the standard of 10 mg/kg, free DOX and drug-loaded nanoparticle solution were injected into tumor-bearing mice by tail vein injection. At the set time (2 h and 6 h after injection), the mice were sacrificed by neck-removal, and the tumor tissues, hearts, livers, spleens, lungs, and kidneys were dissected out for fluorescence intensity detection. Tumor tissues were embedded to make frozen sections, and the distribution of DOX in the tumor was observed by fluorescence microscopy.

In vivo antitumor efficacy

PBS, free DOX, and DOX-P2(NHM)-M were intravenously injected into three groups of tumor-bearing mice every 3 days. The tumor volume and growth status of mice were recorded daily; blood samples were collected at 24 h after the last dose. Fifteen days later, all mice were sacrificed; major organs were washed twice with PBS and immersed in 4% paraformaldehyde solution for 48 h. Samples were dehydrated, embedded in paraffin, and sectioned. Tumor sections were stained with hematoxylin and eosin (H&E), terminal deoxynucleotidyl transferase-mediated UTP nick end labeling (Tunel) staining, and other tissues were stained with H&E.

Safety assessment in vivo

Fifteen healthy Balb/C mice were randomly divided into 3 groups. The first was treated as PBS group; the other two were respectively injected with free DOX and nanoparticle solution with the standard of 5 mg/kg. The growth state and the changes in body weight were recorded. All mice were sacrificed on the 15th day and major organs were dissected out for tissue embedding and sectioning.

Results and discussion

Structural characterization of polymers

FT-IR results of polymers

Taking Fig. 1a as an example, the characteristic functional groups of polymer (black line) were the ester carbonyl (1740 cm^{-1}) and the amide carbonyl (1660 cm^{-1}). The characteristic absorption peak of C-H on benzene ring appears near 3060 cm^{-1}, and the strong peak at 3290 cm^{-1} belongs to the imino group in the backbone peptide bond. The methyl and methylene groups were masked between 2850 and 2940 cm^{-1}, and corresponding absorption peaks at 1360 cm^{-1} and 1472 cm^{-1} were the bending vibration peaks. After the deprotection reaction (red line), the characteristic peak belonging to the benzene ring is obviously weakened, corresponding to a dispersion peak between 2900 and 2500 cm^{-1}, and a strong absorption between 3200 and 3650 cm^{-1}, which are the proof of the appearance of carboxyl group. The peak of amino group from 3300 to 3500 cm^{-1} was masked. After grafting reaction (blue line), the double peak of amino group was exposed between 3420 and 3500 cm^{-1} due to the substitution of a large number of carboxyl groups, and the peak of ester carbonyl group reappeared at 1730 cm^{-1}, and 3470 cm^{-1} is the proof of tertiary amine structure. The peaks of other functional groups can be found in the image. Figure 1b and c differ in peak intensity due to the difference in the ratio of polyglutamic acid to polylysine and the number of side linked branches, and distribution is basically the same.

^{1}H-NMR results of polymers

As shown in Fig. 1d, the characteristic peak of $\delta = 7.95$ ppm is attributed to the N-H of the main peptide bond, and the chemical shift of C-H in the benzene ring of the side chain protection group is between 7.14 and 7.36 ppm. The chemical shift of methylene associated with the benzene ring corresponds to $\delta = 4.96$ ppm. The methylene group in the structure of mPEG is at $\delta = 3.51$ ppm. Other main chemical shifts can correspond to hydrogen in the structure, but the intensity and integral area of the peak are different. In Fig. 1e, due to the electron-absorbing

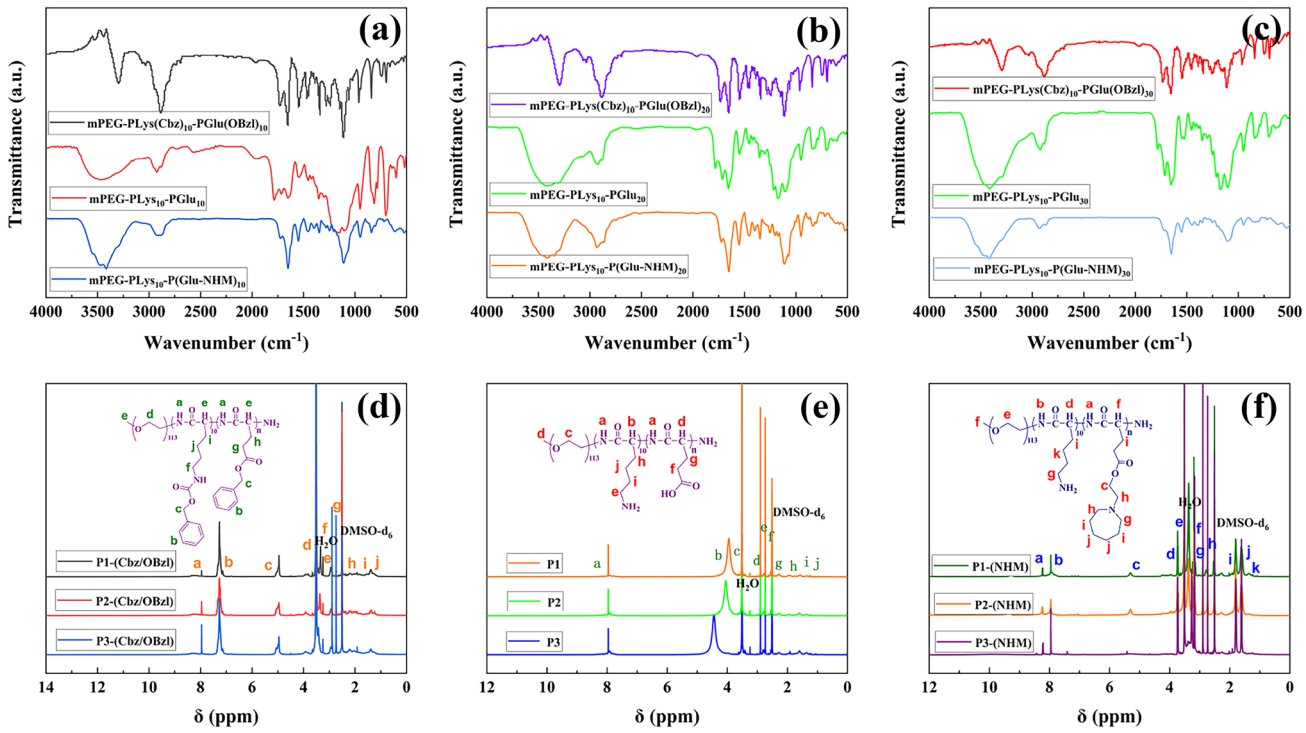

Fig. 1 FT-IR results (**a**–**c**) and ^{1}H-NMR results (**d**–**f**) of synthetic polymers

effect of carboxyl group and the electron-donating effect of amino group, the combined action will affect the chemical shift of C-H. Chemical shifts of C-H on peptide bond were transferred to 3.93 ppm, 4.06 ppm, and 4.46 ppm, respectively. In addition, the characteristic peaks of $\delta = 5.0$ ppm and $\delta = 7.28$ ppm disappeared, which demonstrated that the protective group was smoothly removed. As shown in Fig. 1f, the disappearance of the chemical shift between 4.2 and 3.93 ppm proved that the carboxyl group was substituted. Due to the reappearance of ester group, the characteristic peak of C-H was shifted to 5.28 ppm via strong electron absorption effect. Other chemical shifts $\delta = 2.89$ ppm, $\delta = 2.73$ ppm, $\delta = 1.82$ ppm, and $\delta = 1.61$ ppm were also marked in the spectrum.

GPC results

GPC is used to measure the average molecular mass of materials. Combined with the integral area in ^{1}H-NMR, the results of GPC further confirmed the correctness of the structure of products (see support information S6).

Characterization of drug-loaded nanoparticles

DLS results

It can be seen from Fig. 2a–c, the average particle size were 108.2 nm, 144.3 nm, and 178.2 nm, respectively. With the proportion of polyglutamic acid and the amount of grafting of tertiary amine groups increased, the size becomes larger, which can be understood as a joint result of steric hindrance and charge interactions. The test results of the three nanoparticles are all meet the size requirements in the field of drug sustained release, which is conducive to achieve targeted delivery through EPR effect.

TEM results

The nanoparticles show uniform spherical distribution as shown in Fig. 2d. However, Fig. 2e–f shows an irregular morphology, with the particle size was not uniform and some agglomeration occurred. With the amount of tertiary amine structure increased, the charge repulsion caused the expansion of the volume, and the difference in the length of the molecular chain also resulted in the difference in the size. It is fortunately that the overall particle size is within 200 nm, which is consistent with the results of particle size.

Size stability of nanoparticles

In order to explore the influence of the internal environment on the size changes of the nanoparticles, 10% FBS was added to the solution, and the structural stability was investigated by intermittently testing DLS, as shown in Fig. 2h–j.

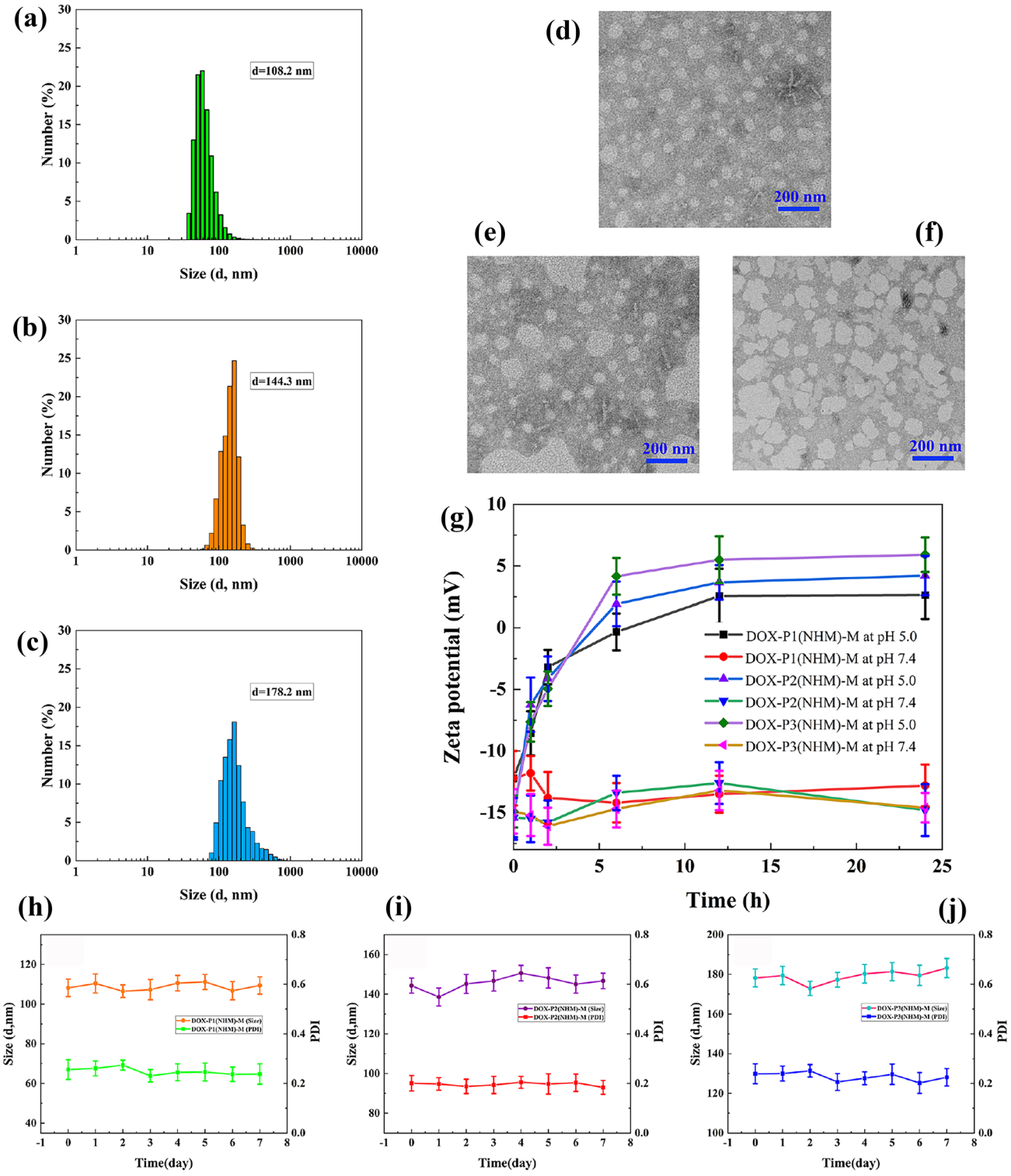

Fig. 2 Size distribution of nanoparticles **a** DOX-P1(NHM)-M, **b** DOX-P2(NHM)-M, **c** DOX-P3(NHM)-M; TEM images **d** DOX-P1(NHM)-M, **e** DOX-P2(NHM)-M, **f** DOX-P3(NHM)-M; **g** zeta-potential changes of nanoparticles after incubation at pH 5.0 or 7.4; size stability of nanoparticles **h** DOX-P1(NHM)-M, **i** DOX-P2(NHM)-M, **j** DOX-P3(NHM)-M

Although the particle size changed due to a small amount of drug release, the overall is within the control range, and the distribution (PDI) has been very uniform. No precipitation was found during the co-culture, which indicated that nanoparticles had good size and structure stability when participating in normal systemic circulation (pH = 7.4).

The change in zeta potential

As shown in Fig. 2g, zeta potential values are different in various environments. Since the surface of cell membrane is negatively charged, nanoparticles can effectively avoid precipitation when participating in normal circulation through electrostatic repulsion. Charge reversal behavior can be achieved through protonation effect of tertiary amine in acidic environment, so as to achieve targeted drug release of nanoparticles. The potential values of DOX-P2(NHM)-M and DOX-P3(NHM)-M changed from − 15.4 mV and − 14.9 mV to 1.93 mV and 4.16 mV, and finally to 4.21 mV and 5.91 mV, which effectively realized the charge reversal. The potential value of DOX-P1(NHM)-M changed from − 12.2 to 2.56 mV at 12 h. The charge reversal mainly depends on the protonation effect of the side-chain tertiary amine structure. DOX-P3(NHM)-M is grafted with the largest amount of NHM, which makes the charge reversal more obvious and rapid.

Drug release behavior of nanoparticles in vitro

Table S1 (supporting information) describes various tests on nanoparticles including LC and LE, and drug release behavior in different environments is explored. As shown in Fig. 3a–c, there is a slow drug release in a neutral environment; the cumulative release rate within 24 h were 40.16%, 36.69%, and 39.59%, respectively, and basically reached equilibrium, which is mainly due to the release of DOX that was mainly coated on the surface of nanoparticles. When pH = 6.2, the release speed was obviously increased, and when pH = 5.0, the cumulative release rates reached 64.8%, 64.28%, and 66.7%, showing an extremely pH sensitivity. The break of imine bonds under acidic conditions destroyed the self-assembly structure and resulted in the release of a large number of drugs. More importantly, the protonation of tertiary amines in acidic environments caused huge charge repulsion, changing morphology to promote drug release.

Due to the rapid proliferation of cancer cells and excessive glycolysis rate, the temperature of internal environment in tumor tissues is slightly higher than normal body. The study of drug release rules at different temperatures is conducive to exploring the structural stability of nanoparticles in different environments, which has guiding significance for the clinical application of drug carriers. As shown in Fig. 3d–f, until the last sampling (90 h), the cumulative release rates of the three materials at 25 °C and 45 °C were

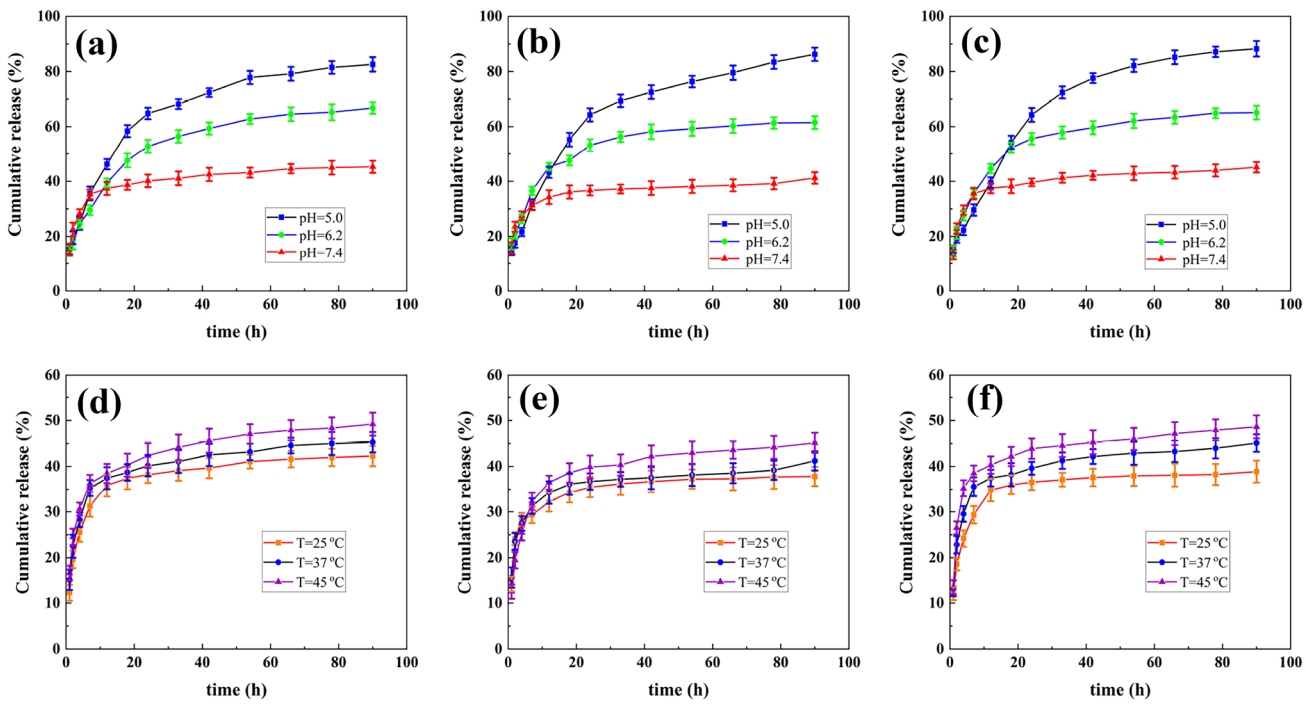

Fig. 3 Cumulative release rate of nanoparticles at different pH **a** DOX-P1(NHM)-M, **b** DOX-P2(NHM)-M, **c** DOX-P3(NHM)-M; and at different temperature **d** DOX-P1(NHM)-M, **e** DOX-P2(NHM)-M, **f** DOX-P3(NHM)-M

42.25% and 49.2%, 37.8% and 45.13%, and 38.88% and 48.6%, respectively. By changing the intramolecular energy and the speed of Brownian motion, drug exudation could be changed. However, the difference was less than 10%, indicating that the release was mainly by physical diffusion, without structural destruction and internal DOX release, which was consistent with the previous results.

Morphology has an important impact on the drug release of nanoparticles. The release kinetics of spherically distributed nanoparticles is often fitted as Korsmeyer-Peppas model [30]. The relevant formulas are as follows:

$$M_t/M_\infty = kt^n \quad (1)$$

$$\log(\frac{M_t}{M_\infty}) = n \log t + \log k \quad (2)$$

Herein, M_t represents the cumulative drug release at time t, M_∞ represents the cumulative drug release over an infinite long period of time, n is the release index related to the release mechanism, and k is the proportionality constant. Where, logarithms are taken from both sides of the equation, and n is the slope value in the fitting data. Generally speaking, when n is below 0.43, drug release is simple diffuse release (type I), also known as Fickian diffusion; when n is above 0.85, the release behavior is mainly caused by the expansion effect of particles (type II). When n is between 0.43 and 0.85, it shows compound release, indicating that the process is jointly acted by the two mechanisms. The kinetic fitting results of cumulative release rate in this experiment are shown in Tables 1 and 2.

According to Table 1, it is surprising to find that the release index is much higher than 0.85 when pH = 5.0, which indicates that drug release behavior belongs to type II release and is mainly achieved through expansion effect of nanoparticles. Under acidic conditions, the protonation effect of tertiary amine causes strong electrostatic repulsion, which increases the volume of nanoparticles, the more PBS buffer can gradually penetrate into the core–shell structure to promote the break of imine bond. This sensitivity gradually decreased with the pH from 6.2 to 7.4, indicating that nanoparticles can respond to the environment clearly and achieve rapid circulation in normal tissues and targeted release in tumor tissues.

Table 1 Related parameters of release kinetics of nanoparticles at different pH

	pH	*n*	*k*	R^2
DOX-P1(NHM)-M	5.0	1	0.0121	0.9993
	6.2	0.8932	0.0192	0.9960
	7.4	0.5277	0.1002	0.9548
DOX-P2(NHM)-M	5.0	1.0729	0.0084	0.9958
	6.2	0.7433	0.0388	0.9897
	7.4	0.4354	0.1455	0.9457
DOX-P3(NHM)-M	5.0	1.0749	0.0084	0.9921
	6.2	0.8201	0.0277	0.9925
	7.4	0.5449	0.0929	0.9236

Table 2 Related parameters of release kinetics of nanoparticles at different temperature

	T	*n*	*k*	R^2
DOX-P1(NHM)-M	25 °C	0.5220	0.0753	0.9512
	37 °C	0.5277	0.1002	0.9548
	45 °C	0.5979	0.1007	0.9633
DOX-P2(NHM)-M	25 °C	0.4269	0.1578	0.9147
	37 °C	0.4354	0.1455	0.9457
	45 °C	0.6301	0.0642	0.9612
DOX-P3(NHM)-M	25 °C	0.5324	0.0858	0.9485
	37 °C	0.5449	0.0929	0.9236
	45 °C	0.5708	0.0989	0.8876

Table 2 shows the relevant parameters at different temperatures, and the release exponent of each group is between 0.43 and 0.85, indicating that the mechanism can be realized by the joint function of type I and type II. The value of n is closer to 0.43 when temperature is low, indicating that drug release is mainly free diffusion. DOX wrapped on the particle surface is a single molecular movement in the initial stage; the release rate tends to be stable in the later stage, which means the influence of temperature is limited.

Cytocompatibility analysis

Cytocompatibility of poly(amino acid)s

The cytocompatibility of polymers was studied by co-culture with L929 cells. Glutamic acid and lysine are both important components in human physiological regulation. NHM, as an important pharmaceutical intermediate, can form a stable ester group on the side chain. As shown in Fig. 4a–c, even if the co-culture concentration was adjusted to 500 μg/mL, the cell survival rate of the all groups of experiments remained above 92%, showing a good affinity for the materials.

Cytocompatibility of nanoparticles

As shown in Fig. 4d, the toxicity of nanoparticles to Hela cells greatly increased with the increase of drug loading. After co-culture for 24 h, the IC_{50} values of DOX-P1(NHM)-M, DOX-P2(NHM)-M, DOX-P3(NHM)-M, and free DOX were 8.23 μg/mL, 4.45 μg/mL, 3.91 μg/mL, and 4.34 μg/mL,

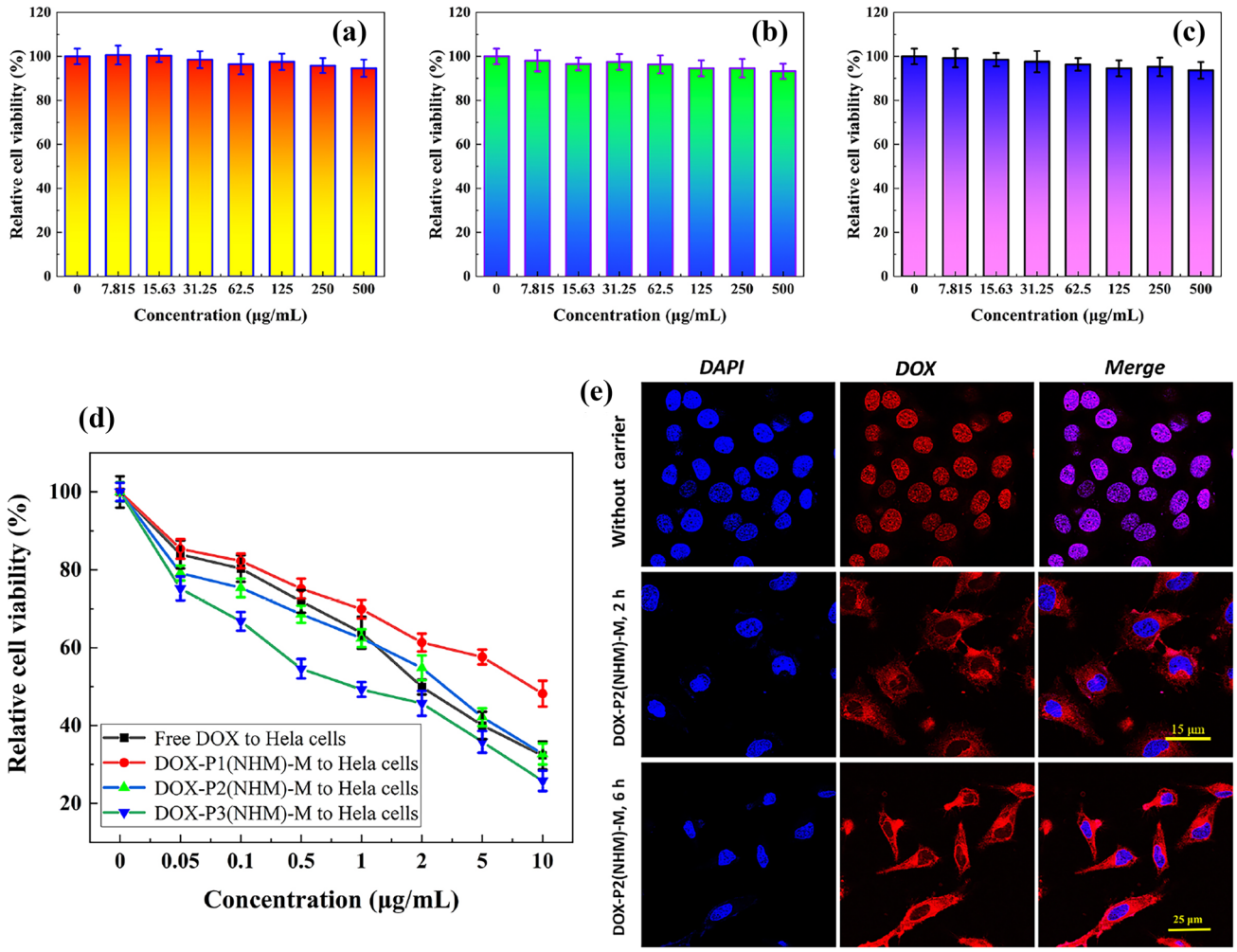

Fig. 4 Cytotoxicity of poly(amino acid)s **a** P1-NHM, **b** P2-NHM, **c** P3-NHM; **d** cellular inhibition of free DOX and nanoparticles; **e** CLSM images of Hela cells after incubation with nanoparticles and free DOX

respectively. On the one hand, more DOX can be released with higher LC when the morphology changed; on the other hand, more tertiary amine structures would result in the particles easier to be taken up by cells through charge reversal.

Cellular uptake behavior of nanoparticles

Figure 4e shows the distribution of fluorescence in cells after 2 h and 6 h of co-cultured, with free DOX (6 h of co-culture) as the reference. Fluorescence of free DOX group only appeared in the nucleus, and the intensity was relatively weak, while the signal was found in both the nucleus and cytoplasm in the nanoparticle group, and the intensity elevated significantly with the prolongation of time. After contact with lysosomes/endosomes, acidic conditions induce charge reversal, which leads to the easier rupture of nanoparticles in the cytoplasm.

Drug distribution in tumor

The distribution of DOX in various organs is shown in Fig. 5a. Fluorescence in the free DOX group was mainly concentrated in the liver and kidney, with a certain intensity in the heart, lung, and spleen, while nanoparticle group was mainly manifested in tumor tissue, and the concentration of the drug increased gradually with the extension of time (from 2 to 6 h). As shown in Fig. 5b, the fluorescence intensity of nanoparticle group at 2 h and 6 h was respectively 1.92 times and 1.68 times than that of the free DOX group, which proved the targeting to tumor tissue.

Figure 5c shows uptake of DOX in tumor tissues. The fluorescence intensities at 2 h were all weaker than that at 6 h, and nanoparticle group was stronger than free DOX group, which is consistent with the results in Fig. 5b. In addition, not only DOX signals were present inside cells, but also a large amount of fluorescence distribution in the extracellular

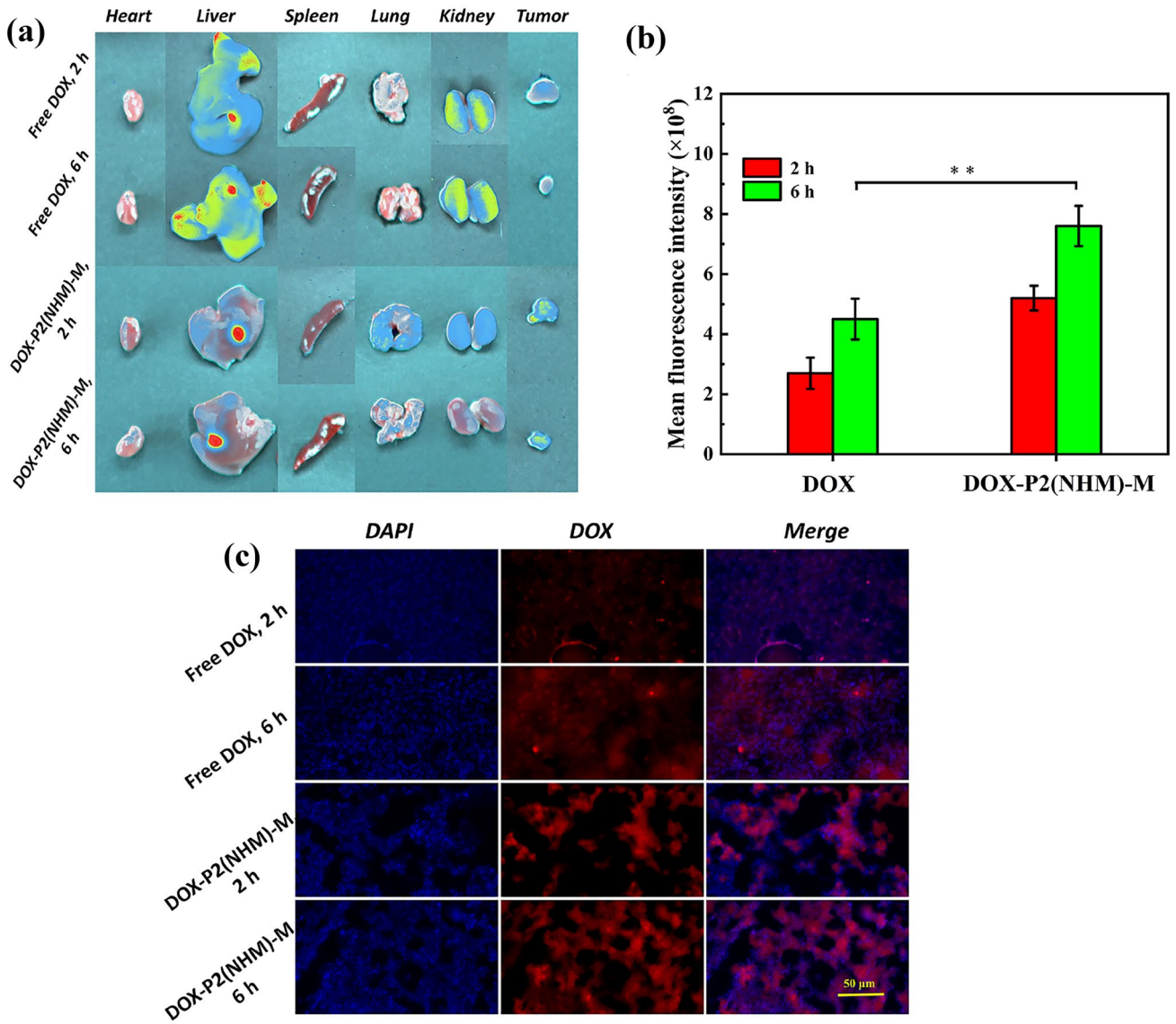

Fig. 5 Ex vivo DOX fluorescence images of main organs and tumors (**a**), and mean fluorescence intensity (**b**) after 2 h or 6 h intravenous injection of free DOX and DOX-P2(NHM)-M into Hela tumors bearing mice, $^{**}p < 0.01$; **c** local fluorescence microscope images of tumor sections, red represents DOX fluorescence, cell nuclei are stained with DAPI (blue)

matrix, indicating that nanoparticles have begun to achieve drug release in the acidic environment inside the tumor.

Tumor inhibition in vivo

DOX, as an exogenous molecule, is easily metabolized by the liver and kidney when participates in systemic circulation. The hydrophilic mPEG shell of nanoparticles can help the encapsulated drugs avoid being metabolized, which is conducive to the retention in tumor tissues through EPR effect.

Antitumor effect

As shown in Fig. 6i, the tumor volume increased uniformly in the PBS group, and the free DOX group showed limited inhibitory effect. The tumor volume of the nanoparticle group was significantly controlled and reduced to half of the original size, indicating that the targeted effect was expressed in the tumor tissue and achieved the release of DOX. Figure 6j describes the relative weight of tumors in each groups, and the results were consistent with Fig. 6i.

Changes of relative body weight can reflect the systemic toxicity to normal body. Figure 6k shows the changes of tumor-bearing mice in each groups within 15 days. The mice in the free DOX group experienced rapid weight loss, mobility difficulties, and lethargy after administration, which indicated that the systemic toxicity was relatively high. The other two groups of mice showed a stable state on the whole, indicating that nanoparticles would not cause injury to the body due to excessive release in the normal systemic circulation.

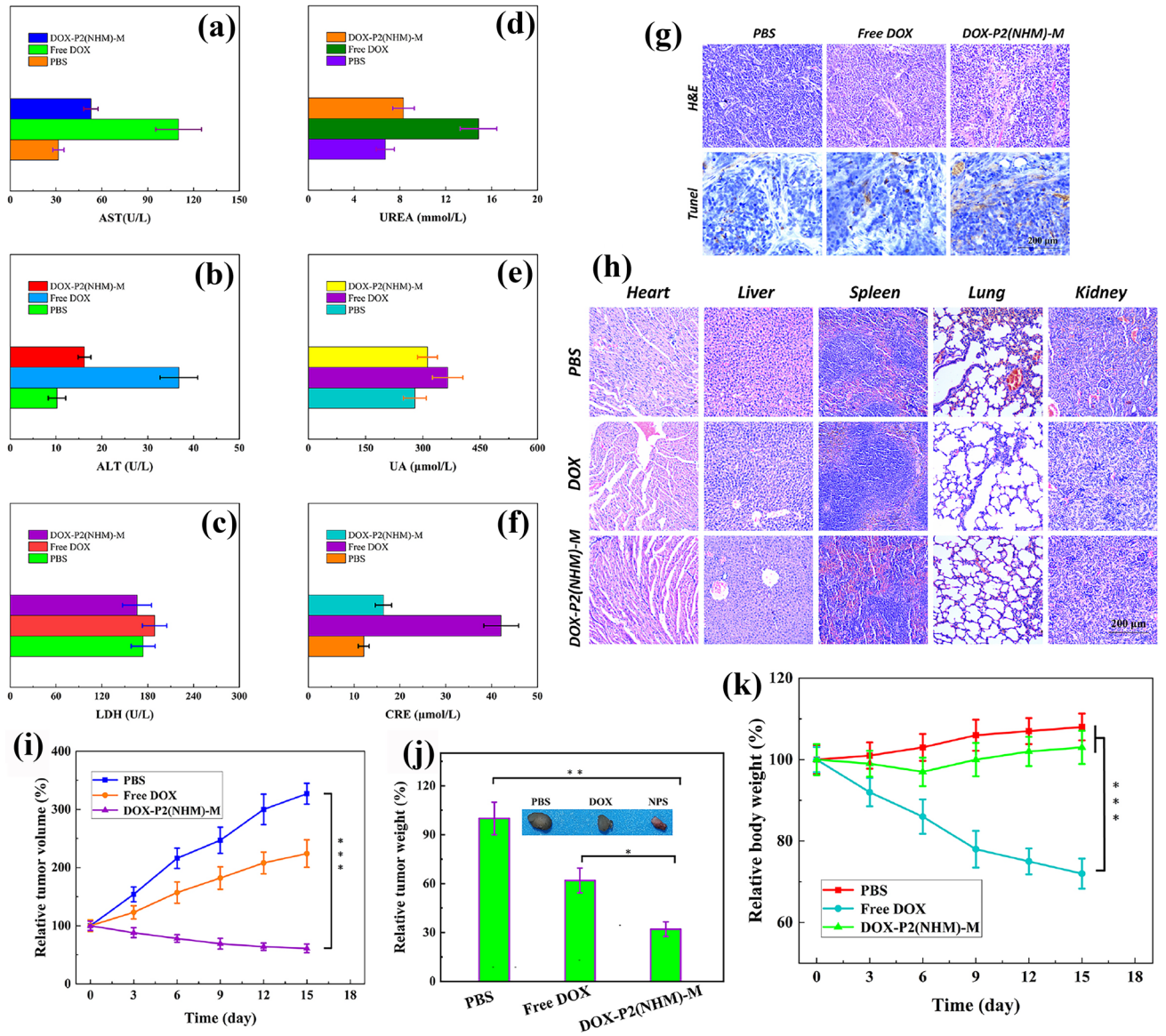

Fig. 6 Blood biochemical analysis of Hela tumor bearing mice after treatment (**a**~**f**); **g** H&E and Tunel analysis of tumor tissues isolated from tumors on 15th day, the scale bar is 200 μm; **h** H&E analysis of major organs after treatments; **i** tumor volume growth curves; **j** relative tumor weights of tumors; **k** relative body weight changes; ***$p<0.001$, **$p<0.01$, *$p<0.05$

Histological analysis of tumor

As shown in Fig. 6g, H&E staining showed that the nuclei of PBS group were polymorphic, the matrix was rich, and the cells were closely packed, indicating that the tumor was in a state of active growth. The density of cell arrangement in free DOX group was decreased but not significantly different from PBS group. The distribution of cells in the nanoparticle group became sparse obviously; some nuclei contracted or broke up and showed large necrotic areas, which was further confirmed by Tunel staining results.

Biochemical analysis of blood after treatment

The blood biochemical test is shown in Fig. 6a–f, and all indexes in free DOX group showed the highest performance among the three groups. This is because free drugs can be quickly digested and metabolized, while DOX has no selective targeting to cells, which affects the function of the liver and kidney. In nanoparticle group, the drug was bonded or wrapped inside the core–shell structure, which can only be released in a specific response, effectively avoiding the side effects on the organs.

Histopathological analysis of major organs

Figure 6h shows the H&E staining results of the major organs after treatment. Compared with PBS group, cardiomyocyte degeneration, glomerular disappearance, and other lesions appeared in the DOX group, and hepatocytes also showed a certain of disorder, indicating that the heart, liver, and kidney had different degrees of systemic toxicity, which was consistent with the results of related blood items. In the nanoparticle group, the cardiomyocytes were intact, the glomeruli were full, and no specific pathological tissue was observed, which avoided the absorption and drug release by other tissues.

Safety assessment in vivo

Safety assessment in vivo is an important index of clinical chemotherapy, which is directly related to the survival and quality of life of cancer patients during treatment. Fig. S4 (support information S7) shows the blood biochemical analysis of healthy Balb/c mice after treatment; the influence of the nanoparticle group on the organs was significantly weakened. In addition, no obvious pathological structure was found in each tissue sections, which indicated that the prepared nanoparticles have a reliable biological safety.

Conclusions

Charge convertible poly(amino acid)s nanoparticles were prepared. The average particle size was between 100 and 200 nm, which meets the conditions for drug release. Drug release showed strong pH sensitivity and showed a mechanism controlled by both free diffusion and expansibility mechanisms. The targeting properties help nanoparticles avoid to be digested or metabolized when participating in systemic circulation. The synthetic polymer is biocompatible and nanoparticles are well ingested by cells via charge reversal. DOX-P2(NHM)-M can treat tumors without causing side effects to normal tissues and organs and have absolute safety in vivo. The prepared nanoparticles have significant targeting function and are expected to be used in biomedicine especially in the field of sustained drug release.

Supplementary Information The online version contains supplementary material available at https://doi.org/10.1007/s13346-023-01323-w.

Acknowledgements This work was sponsored by the Fujian Province University Engineering Research Center of Mindong She Medicine, Ningde Normal University.

Author contribution Zhuang Hu: experimental process, data analysis, manuscript writing. Gongshu Wang: experimental process. Rui Zhang: writing editing. Yingyu Yang: information retrieval. Jiwei Wang: software. Jianshe Hu: supervision, writing-review. Aikebaier Reheman: software.

Funding Fundamental Research Funds for the Central Universities (N2105005) and National Nature Science Foundation of China (31560268).

Availability of data and materials All research data are included in this article or supporting information.

Declarations

Ethics approval and consent to participate All animal experiments were approved by the Northeastern University Medical Ethics Committee.

Consent for publication All the authors agreed to publish the data explored.

Competing interests The authors declare no competing interests.

References

1. Sharma AK, Prasher P, Aljabali AA, Mishra V, Gandhi H, Kumar S, Mutalik S, Chellappan DK, Tambuwala MM, Dua K, Kapoor DN. Emerging era of "somes": polymersomes as versatile drug delivery carrier for cancer diagnostics and therapy. Drug Deliv Transl Re. 2020;10:1171–90.
2. Elbatanony RS, Parvathaneni V, Kulkarni NS, Shukla SK, Chauhan G, Kunda NK, Gupta V. Afatinib-loaded inhalable PLGA nanoparticles for localized therapy of non-small cell lung cancer (NSCLC)-development and in-vitro efficacy. Drug Deliv Transl Re. 2021;11:927–43.
3. Biswas S, Datta LP, Das TK. A bioinspired stimuli-responsive amino acid-based antibacterial drug delivery system in cancer therapy. New J Chem. 2022;46:7024–31.
4. Rahdar A, Hajinezhad MR, Barani M, Sargazi S, Zaboli M, Ghazy E, Baino F, Cucchiarini M, Bilal M, Pandey S. Pluronic F127/doxorubicin microemulsions: preparation, characterization, and toxicity evaluations. J Mol Liq. 2022;345:117028.
5. Fasiku VO, Aderibigbe BA, Sadiku ER, Lemmer Y, Owonubi SJ, Ray SS, Mukwevho E. Polyethylene glycol-gum acacia-based multidrug delivery system for controlled delivery of anticancer drugs. Polym Bull. 2019;76:5011–37.
6. Anderson NM, Simon MC. The tumor microenvironment. Curr Biol. 2020;30:R905–31.
7. Roy DG, Kaymak I, Williams KS, Ma EH, Jones RG. Immunometabolism in the tumor microenvironment. Annu Rev Cancer Biol. 2021;5:137–59.
8. Werfel TA, Cook RS. Efferocytosis in the tumor microenvironment. Semin Immunopathol. 2018;40:545–54.
9. Filipczak N, Joshi U, Attia SA, Fridman IB, Cohen S, Konry T, Torchilin V. Hypoxia-sensitive drug delivery to tumors. J Control Release. 2022;341:431–42.
10. Liu G, Yang L, Chen G, Xu F, Yang F, Yu H, Li L, Dong X, Han J, Cao C, Qi J, Su J, Xu X, Li X, Li B. A review on drug delivery system for tumor therapy. Front Pharmacol. 2021;12:735446.
11. Sun M, Xu X, Lou XF, Du Y. Recent progress and future directions: the nano-drug delivery system for the treatment of vitiligo. Int J Nanomed. 2020;15:3267–79.
12. Yang C, He B, Dai W, Zhang H, Zheng Y, Wang X, Zhang Q. The role of caveolin-1 in the biofate and efficacy of anti-tumor drugs and their nano-drug delivery systems. Acta Pharm Sin B. 2021;11:961e977.
13. Zhang N, Feng N, Xin X, Zhang J, Wu D, Jiang Q, Yu T, Gao M, Zhao S, Yang H, Tian Q. Nano-drug delivery system with enhanced tumour penetration and layered anti-tumour efficacy. Nanomed Nanotechnol. 2022;45:102592.

14. Rajendra PKM, Nidamanuri BSS, Balan AP, Venkatachalam S, Jawahar N. A review on structure, preparation and applications of silk fbroin-based nano-drug delivery systems. J Nanopart Res. 2022;24:141.
15. Guo F, Jiao Y, Du Y, Luo S, Hong W, Fu Q, Li A, Wang G, Yang G. Enzyme-responsive nano-drug delivery system for combined antitumor therapy. Int J Bio Macromol. 2022;220:1133–45.
16. Liu B, Bian Y, Liang S, Yuan M, Dong S, He F, Gai S, Yang P, Cheng Z, Lin J. One-step integration of tumor microenvironment-responsive calcium and copper peroxides nanocomposite for enhanced chemodynamic/ion-interference therapy. ACS Nano. 2022;16:617–30.
17. Dasgupta D, Patel A. A sustainable nano drug delivery system for poorly soluble drug, glipizide: design, in vitro controlled release and kinetics. Mater Adv. 2022;3:8220–28.
18. Yin H, Song P, Chen X, Xiao M, Tang L, Huang H. Smart pH-sensitive hydrogel based on the pineapple peel-oxidized hydroxyethyl cellulose and the Hericium erinaceus residue carboxymethyl chitosan for use in drug delivery. Biomacromol. 2022;23:253–64.
19. Ba S, Qiao M, Jia L, Zhang J, Zhao X, Hu H, Chen D. Construction of hierarchical-targeting pH-sensitive liposomes to reverse chemotherapeutic resistance of cancer stem-like cells. Pharmaceutics. 2021;13:1205.
20. Alhariri M, Majrashi MA, Bahkali AH, Almajed FS, Azghani AO, Khiyami MA, Alyamani EJ, Aljohani SM, Halwani MA. Efficacy of neutral and negatively charged liposome-loaded gentamicin on planktonic bacteria and biofilm communities. Int J Nanomed. 2017;12:6949–61.
21. Zhou Z, Hu F, Hu S, Kong M, Feng C, Liu Y, Cheng X, Ji Q, Chen X. pH-activated nanoparticles with targeting for the treatment of oral plaque biofilm. J Mater Chem B. 2018;6:586–92.
22. Basu A, Kunduru KR, Katzhendler J, Domb AJ. Poly(α-hydroxy acid)s and poly(α-hydroxy acid-co-α-amino acid)s derived from amino acid. Adv Drug Deliver Rev. 2016;107:82–96.
23. Wang S, He W, Xiao C, Tao Y, Wang X. Synthesis of Y-shaped OEGylated poly(amino acid)s: the impact of OEG architecture. Biomacromol. 2019;20:1655–66.
24. Tian J, Jiang R, Gao P, Xu D, Mao L, Zeng G, Liu M, Deng F, Zhang X, Wei Y. Synthesis and cell imaging applications of amphiphilic AIE-active poly(amino acid)s. Mat Sci Eng C. 2017;79:563–9.
25. Fan X, Zhu S, Yan L, Zhu H. Reactive oxygen species-responsive degradable poly(amino acid)s for biomedical use. J Appl Polym Sci. 2021;138:e51386.
26. Hu Z, Wang J, Han S, Hu J, Reheman A. Self-assembly behavior and sustained drug release properties of amphiphilic poly(amino acid)s. New J Chem. 2022;46:19888.
27. He W, Tao Y. Bifunctional fluoroalcohol catalysts enabled sustainable synthesis of poly(amino acid)s. Chin J Chem. 2021;39:2119–24.
28. Temimi AHKA, Martin M, Meng Q, Lenstra DC, Qian P, Guo H, Weinhold E, Mecinovic J. Lysine ethylation by histone lysine methyltransferases. Chem Bio Chem. 2020;21:392–400.
29. Yu A, Lau AY. Energetics of glutamate binding to an ionotropic glutamate receptor. J Phys Chem B. 2017;121:10436–42.
30. Colombo P, Bettini R, Catellani PL, Santi P, Peppas NA. Drug volume fraction profile in the gel phase and drug release kinetics in hydroxypropylmethyl cellulose matrices containing a soluble drug. Eur J Pharm Sci. 1999;9:33–40.